This is a peer-reviewed, accepted author manuscript of the following research article:
Ashraf, K. U., Josts, I., Mosbahi, K., Kelly, S. M., Byron, O., Smith, B. O., & Walker, D. (2016). The potassium binding protein Kbp is a cytoplasmic potassium sensor. Structure, 24(5), 741-749. https://doi.org/10.1016/j.str.2016.03.017

The Potassium Binding Protein Kbp is a Cytoplasmic Potassium Sensor

Khuram U. Ashraf[1‡], Inokentijs Josts[2‡], Khedidja Mosbahi[2‡], Sharon M. Kelly[1], Olwyn Byron[3], Brian O. Smith[1]*, Daniel Walker[2]*

[1] Institute of Molecular Cell and Systems Biology, College of Medical, Veterinary, and Life Sciences, University of Glasgow, Glasgow G12 8QQ, United Kingdom
[2] Institute of Infection, Immunity and Inflammation, College of Medical, Veterinary and Life Sciences, University of Glasgow, Glasgow G12 8QQ, United Kingdom
[3] School of Life Sciences, College of Medical, Veterinary and Life Sciences, University of Glasgow, Glasgow G12 8QQ, United Kingdom

* To whom correspondence should be addressed: E-mail: Brian.Smith@glasgow.ac.uk or Daniel.Walker@glasgow.ac.uk

‡These authors contributed equally.

Abstract

E. coli possesses a number of specific K^+ influx and efflux systems that maintain an appropriate intracellular K^+ concentration. Although regulatory mechanisms have been identified for a number of these transport systems, the exact mechanism through which K^+ concentration is sensed in the cell remains unknown. In this work we show that Kbp ($\underline{K}^+$ binding protein, formerly YgaU), a soluble 16 kDa cytoplasmic protein from *E. coli*, is a highly specific K^+ binding protein and is required for normal growth in the presence of high levels of external K^+. Kbp binds a single potassium ion with high specificity over Na^+ and other metal ions found in biological systems, although, in common with K^+ transporters, it also binds Rb^+ and Cs^+. Dissection of the K^+ binding determinants of Kbp suggests a mechanism through which Kbp is able to sense changes in K^+ concentration over the relevant range of intracellular K^+ concentrations.

Introduction

Potassium is the major intracellular cation and is concentrated in the cytoplasm by transport systems that have a high specificity for K^+ over other monovalent cations such as Na^+. Due to the central role of K^+ in key homeostatic mechanisms such as maintenance of intracellular pH and osmolarity, the cytoplasmic K^+ concentration is closely controlled (Booth, 1985; Weiden et al., 1967). However, despite the identification and detailed characterisation of K^+ transporters and channels in *Escherichia coli*, our understanding of how intracellular levels of K^+ are sensed and how an appropriate K^+ concentration is maintained is incomplete. For bacteria such as *E. coli*, which are able to colonise a range of environments that vary widely in pH, osmotic potential regulating the intracellular K^+ concentration is likely to provide a significant challenge.

In the cytoplasm of *E. coli* during normal growth the K^+ concentration is approximately 250 mM, although this may vary significantly depending on exact environmental conditions (Weiden et al., 1967). Potassium influx forms a primary response upon osmotic upshock as bacterial cells begin to lose turgor pressure due to the efflux of water. The accumulation of potassium glutamate inside the cytosol leads to several adaptive changes resulting in the reprogramming of cellular gene expression profiles, transport and *de novo* synthesis of neutral osmoprotectants. Changes to cellular transcription have been shown to be mediated directly by potassium glutamate which is able to directly inhibit RNA polymerase (Gralla and Vargas, 2006). In addition, potassium glutamate has been shown to directly stimulate transcription from an RpoS-dependent promoter (Lee and Gralla, 2004). The RpoS regulon in *E. coli* consists of a number of stress response genes which are up-regulated by osmotic stress (Vijayakumar et al., 2004).

E. coli contains a number of K^+ transport systems, with active uptake mediated by the Trk, Ktr and Kup transporters and active efflux by the Kef transporter (Bossemeyer et al., 1989a; Bossemeyer et al., 1989b; Nakamura et al., 1998; Roosild et al., 2010). In addition, Kch, an *E. coli* homologue of eukaryotic K^+ channels, has been shown to form an active potassium conducting channel *in vivo*, although the physiological conditions under which the activity of K^+ channel is required have not been established (Kuo et al., 2003). K^+ transport systems are able to readily discriminate between K^+ and Na^+, which differ in radius by only 0.38 Å, and the basis for the specificity of K^+ channels has been widely investigated, both experimentally and theoretically (Doyle et al., 1998; Noskov and Roux, 2006; Yu et al., 2010; Zhou et al., 2001).

The cytoplasmic protein Kbp ($\underline{K}^+$ binding protein, formerly YgaU) from *E. coli* is one of a small number of proteins that are strongly induced in response to osmotic stress, due to the addition of sodium chloride, and is a member of the RpoS regulon (Vijayakumar et al., 2004). Kbp is a 16 kDa protein that is predicted to be located in the cytoplasm and contains an N-terminal BON (bacterial OsmY and nodulation) domain and a C-terminal LysM (lysin motif) domain. The LysM domain is frequently associated with peptidoglycan binding and changes in the cellular level of Kbp (YgaU) have been shown to modulate peptidoglycan cross-linking (Bateman and Bycroft, 2000; Bernal-Cabas et al., 2015). The BON domain is predicted to be a membrane-associated phospholipid binding domain although the experimental evidence to support this assertion is controversial (Teriete et al., 2010; Yang et al., 2011; Yeats and Bateman, 2003). However, there is direct experimental evidence that Kbp is peripherally associated with the cytoplasmic face of the inner membrane (Papanastasiou et al., 2013). BON domains are predicted for two other *E. coli* proteins; OsmY and YraP. Although the exact roles of these proteins are not fully understood, expression levels of OsmY are upregulated in response to osmotic stress and YraP is an

outer membrane lipoprotein that is likely involved in outer membrane biogenesis (Onufryk et al., 2005; Yim and Villarejo, 1992). In this work we show that the cytoplasmic protein Kbp is required for normal growth in the presence of K^+ concentrations in excess of 1 mM and under conditions of salt-induced osmotic stress. Biophysical and structural analysis shows that Kbp binds a single potassium ion and that K^+ binding induces a large conformational change in the protein. The isolated BON domain is able to bind potassium with an affinity of approximately 20 mM, suggesting a mechanism by which Kbp may act as a sensor of cytoplasmic K^+ concentration.

Results

Kbp is a K^+ binding protein

In *E. coli,* elevated levels of Kbp have been reported in response to osmotic stress associated with high levels of sodium chloride (0.4 M), but not organic osmolytes (Weber et al., 2006). Additionally, *kbp* (*ygaU*) has been shown to be regulated by the alternative sigma factor RpoS that regulates the expression of many stress response genes (Vijayakumar et al., 2004). These results suggest that Kbp may serve a key role in adaptation and stress responses.

Our initial experiments showed that Kbp could be readily overexpressed in *E. coli* BL21(DE3) and purified by nickel affinity chromatography and gel filtration. Gel filtration indicated that this protein was present as a single species that eluted at a position consistent with the protein being monomeric. However, ^{15}N-heteronuclear single-quantum coherence (HSQC) spectra of ^{15}N labelled Kbp purified by gel filtration and recorded in 20 mM sodium phosphate pH 7.2 were poorly resolved with fewer than the expected number of crosspeaks, and with broad linewidths and a lack of chemical shift dispersion for many of the peaks that remained, indicating that a significant proportion of Kbp lacks a well-defined 3D structure under these conditions (**Figure 1a**). Serendipitously, we discovered that spectra recorded in buffer containing potassium ions were well dispersed and well resolved with crosspeaks of uniform lineshape, indicating that K^+ ions are required to stabilise Kbp structure (**Figure 1b**). Thus, spectra recorded in sodium phosphate buffer with 5 mM KCl were well dispersed, but those recorded with even 250 mM Na^+ were not. In addition, differential scanning calorimetry (DSC) showed a marked increase in the thermodynamic stability of Kbp in the presence of K^+ and far- and near-UV CD spectra of Kbp recorded in the presence and absence of K^+ also indicated that Kbp undergoes significant structural changes on K^+ binding (**Figure 1cde**).

To further investigate the binding of K^+ and other monovalent cations by Kbp we performed isothermal titration calorimetry (ITC) experiments. Titration of KCl into a solution of Kbp in 50 mM Tris, 50 mM NaCl pH 7.5 at 298 K showed that formation of the Kbp-K^+ complex is enthalpy driven, ΔH = -9.8 kcal mol^{-1}, and entropically disfavoured, $T\Delta S$ = -4.6 kcal mol^{-1} (**Figure 1f**). This is consistent with ordering of the Kbp structure on K^+ binding inferred from our NMR and DSC experiments. The K_d for the Kbp-K^+ complex is approximately 160 µM with a single K^+ binding site per Kbp molecule (**Table S1**). No detectable heats of binding were observed on titration of sodium chloride into Kbp in 50 mM Tris, 50 mM LiCl pH 7.5. Taken together with the data presented in Figure 1, this suggests that Kbp has little affinity for Na^+. Thus, Kbp is able to effectively discriminate between K^+ and the chemically similar, but smaller alkali metal ion, Na^+. ITC experiments with the larger alkali metal ions Rb^+ and Cs^+ showed that Kbp forms a complex with both these ions, with the affinity of Kbp for Rb^+ similar to that of K^+, and the affinity for Cs^+ more than 10-fold lower (**Figure S1, Table S1**). ITC studies with the K^+ channel, KcsA, from *Streptomyces lividans*

have shown that this protein displays an affinity for K^+ similar to Kbp. In addition, KcsA was shown to bind Rb^+ and Cs^+ but not Na^+ (Lockless et al., 2007). The soluble protein Kbp therefore displays a cation-specificity similar to that of a K^+ channel. Outside the alkali metal ions, Kbp binds NH_4^+ which is also a substrate of potassium channels, with an affinity close to that for Cs^+ (**Figure S1, Table S1**). However, ITC was unable to detect any heat associated with binding on titration of the primary amine containing compounds spermidine and putrescine.

Additionally, we monitored K^+ association with Kbp under pseudo-first-order conditions using stopped-flow fluorimetry in order to follow the rate of Kbp-K^+ complex formation. Mixing Kbp with excess KCl resulted in the quenching of intrinsic Trp fluorescence (**Figure S2a**). The data were fitted with a single-exponential model, with k_{obs} increasing linearly with increasing KCl concentration indicating that k_{obs} describes the bimolecular association step (**Figure S2b**). Values for the association rate constant (k_{on}) and dissociation rate constant (k_{off}) of 6.27 ± 0.15 x10^4 M^{-1} s^{-1} and 7.89 s^{-1} were determined, respectively, from a plot of k_{obs} vs [KCl] (**Figure S2b**). Calculation of K_d for the Kbp-K^+ complex from the ratio k_{off}/k_{on} gave a value of 126 µM which agrees closely with the value determined by ITC under the same conditions. The dissociation rate constant showed little variation with increasing ionic strength to 0.3 M NaCl (8.97 s^{-1}) and a 3-fold increase with 0.6 M NaCl (17.3 s^{-1}). However, we saw a large decrease in the association rate constant with increasing ionic strength: k_{on} was reduced to 2.0 x10^4 M^{-1} s^{-1} in 0.3 M NaCl and 5.7 x10^3 M^{-1} s^{-1} in 0.6 M NaCl (**Figure S2bc**). Consequently, the K_d of the Kbp-K^+ complex increases approximately 30-fold on increasing the salt concentration from 50 mM to 600 mM NaCl with K_d values of 0.1 mM, 0.4 mM and 3mM determined by stopped-flow fluorimetry at 50, 300 and 600 mM NaCl, respectively. Thus, at high ionic strength, which may better represent physiological conditions, the K_d for the Kbp-K^+ complex is considerably higher than at low ionic strength.

Kbp is required for normal growth at a range of elevated K^+ concentrations

Since we have established that Kbp is a K^+ binding protein and its production has previously been shown to be upregulated on osmotic stress with NaCl we hypothesised that the soluble cytoplasmic protein Kbp could be directly involved in K^+ homeostasis. Despite intensive research into K^+ transport, no protein has been identified that is a direct sensor of cytoplasmic K^+ concentration. To determine if Kbp is involved in K^+ homeostasis we compared the ability of the wild-type and *Δkbp* strains to grow at a variety of K^+ concentrations in a defined sodium phosphate-based minimal medium with KCl added at a range of concentrations. At low K^+ concentrations (0.05 and 0.01 mM KCl) there was no difference in the growth rates of the wild-type and *Δkbp* strains (**Figure S3**). At higher K^+ concentrations (1, 5 and 50 mM) the wild-type strain showed little variation in growth rate with K^+ concentration (**Figure 2**). However, the *Δkbp* strain showed a delay of around 2 hours in entering exponential phase at 1 mM KCl and a delay of around 5 hours at 5 and 50 mM KCl. Thus the loss of Kbp delays growth with increasing K^+ concentration (1-5 mM). Taken together, the specific binding of K^+ by Kbp and the K^+ sensitive growth phenotype of cells lacking Kbp suggests that this cytoplasmic protein likely plays a key role in K^+ homeostasis, perhaps sensing cytoplasmic K^+ concentration. However, the K_d for the Kbp-K^+ complex seems incompatible with a role in cytoplasmic K^+ sensing where the concentration of K^+ is typically around 200 mM. One possibility is that that the affinity of Kbp for K^+ is modulated by protein-protein interactions or a competing non-protein ligand.

Full K^+ binding requires both the BON and LysM domains of Kbp

To begin to dissect the K^+ binding determinants of Kbp we purified the isolated BON and LysM domains of Kbp. Near-UV CD indicated that the isolated BON domain undergoes a conformational change in the presence of K^+ whereas the isolated LysM domain does not (**Figure S4**). In addition, ITC showed enthalpically driven complex formation between the BON domain and K^+, whereas no heat was liberated on titration of KCl with the isolated LysM domain (**Figure S4**). However, ITC also indicated that K^+ forms a substantially weaker complex with the isolated BON domain than with Kbp. The estimated K_d for the BON-K^+ complex is $\geq$ 20 mM, in excess of 100-fold greater than for the Kbp-K^+ complex (160 μM), suggesting that although the major interaction site lies within the BON domain, further interactions that stabilise the complex of K^+ with Kbp involve its LysM domain. To monitor the conformational changes that the BON domain undergoes on K^+ binding, we produced ^{15}N labelled BON domain and monitored the changes to its ^{15}N-HSQC spectra upon the addition of K^+. In the absence of K^+, ^{15}N-HSQC spectra of the BON domain were poorly resolved indicating that the isolated domain is largely unfolded. However, on addition of K^+, the ^{15}N-HSQC spectra improved, and at 270 mM K^+ were well dispersed, indicative of a folded protein (**Figure S4**). In intact Kbp, residues in both the BON and LysM domains shift on K^+ addition. Taken together, these data indicate that the major K^+ binding site is located in the BON domain and this initial complex is stabilised by interaction with the LysM domain.

Solution Structure of Kbp-K^+

To attempt to gain further insight into K+ binding by Kbp, we determined the structure of K^+-saturated Kbp in solution by NMR spectroscopy (**Figure 3, Table 1**). Kbp-K^+ forms a compact, globular, heart-shaped structure (approximate dimensions 50 Å wide by 40 Å high by 30 Å deep) with the BON and LysM domains packed against one another. The N-terminal BON domain (residues 23-91) adopts an α-β-β-α-β topology forming a three-stranded mixed β-sheet with alpha helix αB linking the second and third parallel strands, as seen in other BON domains (Teriete et al., 2010; Yang et al., 2011) (also PDB:4qo6). However, the third strand is perturbed at N86 in order to accommodate a hydrogen-bond between the amide of V87 and the side-chain of D85. Alpha helix αA (residues 24-38) packs across the C-terminal ends of the first strand and is joined to the first strand by a linker that incorporates another helical turn. Residues 1-23 augment the BON domain structure, with residues 2-6 forming a fourth, short β-strand antiparallel to residues 81-85, and residues 7-23 forming a stretch of irregular structure that encloses the loop formed by residues 76-80. Residues 96-149 form a structure similar to those of previously determined LysM domains (Bateman and Bycroft, 2000; Bielnicki et al., 2006; Koharudin et al., 2011; Sanchez-Vallet et al., 2013), with a two-stranded antiparallel β-sheet enclosing one side of a small hydrophobic core whose other side is bounded by two, almost perpendicular alpha helices. However, the linker from the second helix of the LysM domain to the C-terminal β-strand in Kbp lacks any of the helical character seen in this part of other LysM domains.

The two domains are tethered to one another by a short, ordered linker (residues 90-95) that caps the N-terminus of αB, with a hydrogen bond forming between the amide group of Gln 64 and the carbonyl of Thr 91. The LysM domain packs principally against the opposite side of αB from the BON domain's β-sheet, with the LysM β-sheet facing the BON domain forming additional contacts to the N-terminal strand, the C-terminal end of αA and its adjacent loop. The interface between the domains is maintained by a hydrophobic core involving F4, F6, T38, I40, L71, V72 and A73 from the BON and F98, T100, P130, M131 and V143 from the LysM domains respectively. In addition there is a buried salt bridge between

E65 and R145 close to the inter-domain linker, while at the other end of the interface, N76 forms two hydrogen bonds to the backbone of V143 and Q142 is sandwiched between N76 and Y139. Q142, N76 and Y139 line the sides of a small pocket between the domains that is also bounded by E12, H34, M131, L132 and K133.

Comparison of Kbp-K^+ and apo-Kbp

To determine the extent of conformational changes in the context of the whole protein on K^+ binding we used small angle X-ray scattering (SAXS) and sedimentation velocity analytical ultracentrifugation data to model apo-Kbp and K^+-bound Kbp. High quality SAXS data were acquired for a range of concentrations of Kbp in the presence and absence of K^+ (**Figure 4a**). Guinier analysis of these data revealed a significant change in the radius of gyration (R_g): 2.28 nm for the apoprotein and 1.79 nm for the K^+ bound form. The reduction in R_g suggests a marked compaction of the overall Kbp structure upon K^+ binding. The p(r) function describes the paired set of distances between all the electrons within the protein and allows detection of any conformational changes (here, in response to K^+). The maximum particle diameter (D_{max}) of Kbp in the presence of K^+ (6.5 nm) was determined from the indirect Fourier transformation of the experimental data (**Figure 4b**). The plot for Kbp-K^+ is characterised by a bell-shaped curve peaking at around $D_{max}/2$, indicative of a globular protein. In contrast, the apo-Kbp curve reveals some globularity with an extended tail region giving rise to higher r values, suggesting that the apoprotein is less globular in shape and may include an extended region. The D_{max} of apo-Kbp is 12.5 nm (**Figure 4b**). Foldedness and flexibility of Kbp in the presence and absence of K^+ was further analysed by inspecting the normalised Kratky plot, which reports on a molecule's compactness and overall flexibility (Durand et al., 2010). In the normalised Kratky plot, fully folded, globular proteins present a bell-shaped curve with a maximum close to 1.1. Kbp-K^+ possesses a maximum at approximately 1.36, indicative of globularity. In the case of apo-Kbp the peak maximum is shifted to the right (1.86) which, taken together with the increased area under the curve, indicates a non-globular, asymmetric character with substantial conformational heterogeneity within the protein (**Figure 4c)**. SAXS data obtained for Kbp in the presence and absence of K^+, were used to reconstruct low-resolution solution structures. *Ab initio* models were generated for each of apo-Kbp and Kbp-K^+ using GASBOR (Svergun et al., 2001) and within these, similar models were combined into an average model for each form of Kbp using DAMAVER (Volkov and Svergun, 2003) (**Figure 4d**).

To validate our structural models of both the high-resolution structure and *ab initio* generated models of Kbp-K^+ the protein was subjected to hydrodynamic analysis using SOMO bead modelling and analytical ultracentrifugation experiments (Brookes et al., 2010) (Rai et al., 2005). Consistent with the SAXS data, which show a decrease in R_g upon K^+ binding, sedimentation velocity experiments showed that K^+ binding was associated with global structural changes in Kbp, with the Kbp-K^+ complex ($s^0_{20,w}$ = 1.90 S sedimenting considerably faster than apo-Kbp ($s^0_{20,w}$ = 1.56 S) due to a decrease in the frictional coefficient of the molecule (**Figure S5, Table S2**). Experimentally obtained hydrodynamic parameters of Kbp were close to those derived from computed bead models of apo-Kbp and Kbp-K^+ generated from SAXS *ab initio* models, validating these models (**Table S2**). Taken together, the SAXS and sedimentation velocity experiments suggest that Kbp undergoes a substantial compaction upon association with K^+, possibly as a consequence of BON domain folding/ ordering in the context of the entire molecule.

Discussion

In this work we have shown that Kbp is an unprecedented, soluble K^+ binding protein that is required by *E. coli* for normal growth at high levels of external K^+. Kbp selectively binds a single K^+ (radius = 1.33 Å) and larger alkali metal ions such as Rb^+ (radius = 1.48 Å) and Cs^+ (radius = 1.69 Å) but does not readily bind the smaller Na^+ ion (radius = 0.95 Å), and in this respect has an ion specificity similar to that of K^+ channels (Lockless et al., 2007). Kbp binds Rb^+ with only slightly reduced affinity, but binding of the larger Cs^+ ion is approximately an order of magnitude weaker. Binding of alkali metal ions is associated with a specific conformational change in Kbp, with NMR data indicating that in the absence of K^+ Kbp is partially unfolded. This is consistent with DSC experiments which show a significant increase in the enthalpy of unfolding on K^+ binding. Taken together with the phenotype of cells lacking Kbp, which display retarded growth at high potassium concentrations, the ability to selectively bind K^+ suggests a role in potassium homeostasis. The phenotype of growth inhibition of cells lacking Kbp at high concentrations of K^+ is remarkably similar to the phenotype displayed by gain-of-function mutants of the *E. coli* K^+ channel, Kch (Kuo et al., 2003). These mutations are located in the cytoplasmic sensor domain of Kch and when mapped onto the structure of this domain form a putative ligand/protein binding site. Therefore one possible explanation for the K^+ sensitivity of the *Δkbp* strain is that Kbp is the regulatory protein of a potassium transport system.

Expression of the isolated domains showed that the BON domain retains the ability to bind K^+, although with approximately 100-fold reduced affinity. Binding to the isolated LysM domain could not be detected. We therefore infer that, although the majority of groups involved in K^+ binding are located in the BON domain, residues in the LysM domain must also be important in stabilising the Kbp-K^+ complex. Our data also suggest that the conformational change on K^+ binding occurs predominantly in the BON domain, with NMR showing that in the absence of K^+ the isolated BON domain is largely unfolded. The highly specific binding of K^+ to an essentially unfolded region of polypeptide suggests that K^+ specificity is determined in a way that is fundamentally different from that observed for K^+ channels. In these membrane-bound channels, K^+ binding sites are formed from backbone carbonyl groups from regions of polypeptide held in an unusual α-sheet conformation within the rigid constraints of the channel (Zhou et al., 2001). High resolution structures of the K^+ channel Ksc show K^+ coordinated in the narrow selectivity filter by eight backbone carbonyl groups of the tetrameric transporter. It is thought that this topological arrangement is optimal for coordination of K^+ and can therefore compensate for the energetic cost of desolvation on binding and transport (Bostick and Brooks, 2007). Selectivity for K^+ over the smaller Na^+ is imparted as this topological arrangement does not effectively coordinate the smaller Na^+ to the extent that the energetic penalty of desolvation cannot be adequately compensated. Outside the structural constraints of a channel there is little known about how soluble proteins are able to selectively bind K^+ in preference to Na^+. Our analysis of Kbp, even in conjunction with sequence comparison between Kbp homologues, does not yet reveal where K^+ binds and our work continues in this area.

Although we do not yet understand why Kbp is required for growth in media containing high levels of K^+, one possibility is that it is acting as a direct sensor of cytoplasmic K^+ concentration that subsequently enables adaptation to these conditions. The concentration of K^+ in the cytoplasm of *E. coli* is typically 200 mM but can vary significantly, for example under osmotic stress. Additionally, although the total concentration of K^+ within the cytoplasm can be directly measured there is considerable uncertainty as to how much of this exists in the free rather than bound form as the cytoplasm contains numerous species

such as nucleic acids, phospholipids, protein and small molecule metabolites with an affinity for K^+. In addition, ^{39}K NMR data suggest that up to 50% of cytoplasmic K^+ may be in the bound form that is invisible to NMR (Richey et al., 1987). Clearly, if K^+ were the only ligand of Kbp, a K_d of 160 μM would preclude Kbp from this role since at all feasible cytoplasmic K^+ concentrations, Kbp would be present only in the bound form. In addition, given the high level of selectivity for K^+ it seems unlikely that an alternative ligand would directly compete with K^+ for binding at the K^+ binding site. However, if the LysM domain of Kbp is bound by a competing ligand and therefore cannot participate in stabilisation of the BON domain-K^+ complex then the affinity of Kbp for K^+ may be reduced to that of the isolated BON-K^+ complex, which has a K_d of approximately 20 mM. Given the total concentration of K^+ in the cytoplasm of *E. coli* is approximately 200 mM and there are high concentrations of competing ligands in the cell which will bind potassium, albeit with relatively low affinity, this is likely to be of the correct order of magnitude for a useful cytoplasmic K^+ sensor.

One possible mechanism through which Kbp may regulate cation homeostasis is suggested by recent data indicating that the gene encoding Kbp and the downstream gene *yqaE*, which encodes a small membrane protein are cotranscribed under conditions that induce the Cpx envelope stress response (Bernal-Cabas et al., 2015). Although the function of YqaE has not been elucidated, homologous proteins in yeast and plants, Pmp3 and RCI2 proteins, respectively, have been shown to play a key role in cation homeostasis and in particular the regulation of intracellular Na^+ and K^+ levels (Medina et al., 2001; Rocha, 2016). Thus, given the genetic link between the genes encoding Kbp and YqaE it is reasonable to speculate that in *E. coli*, Kbp functions as a regulator of YqaE, which may act as a cation transporter and under stress conditions play a role in cation homeostasis.

Materials and Methods

Cloning and purification

Plasmid pKA1 was produced to express Kbp with a C-terminal His_6-tag (Kbp_{His6}). To construct pCM6, *Kbp* from *E. coli* K-12 BW25113 was amplified using primers YgaUF (GGA ATT CCA TAT GGG TCT GTT CAA TTT TGT GAA AG) and YgaUR (CCG CTC GAG CTC TTC CGG AAT ACG CAA CAC TTG), the PCR product was digested with NdeI and XhoI and introduced into the corresponding sites of pET21d (Novagen). Kbp_{His6} was overexpressed from *E. coli* BL21(DE3) carrying the plasmid pKA1. 5 L of LB broth was inoculated (1:100) and overnight culture and cells were grown at 37°C in a shaking incubator to an OD_{600} = 0.6. Protein production was induced by the addition of 1 mM IPTG, the cells were grown for a further 3 hours and harvested by centrifugation. The cell pellet was resuspended in 20 mM Tris-HCl and 500 mM NaCl containing 5 mM imidazole (pH 7.5). Cells were lysed using a MSE Soniprep 150 (Wolf Laboratories, UK) and the cell debris separated by centrifugation. The cell-free lysate was applied to a 5 ml His Trap™ HP column (GE Healthcare, USA) and the protein eluted over a 0-350 mM imidazole gradient. Kbp_{His6}-containing fractions were dialysed overnight into 50 mM Tris-HCl, 50 mM NaCl (pH 7.5) and the protein was further purified by gel filtration chromatography on a Superdex S75 26/60 column (GE Healthcare) equilibrated in 50 mM Tris-HCl, 50 mM NaCl (pH 7.5). The protein was stored at -20°C in this buffer until required. For expression of the isolated Kbp BON domain (residues 1-89) plasmid pIJ1 was engineered by the introduction of an XhoI site in *kbp* from pKA1, digestion with XhoI to excise the XhoI fragment and religation of the vector with T4 DNA ligase after gel purification. Site directed mutagenesis of pAK1 to introduce an XhoI site was performed using the Stratagene quick change method with primers XhoIF (GTC GAT GAT CAG GTG AAA ACG CTC GAG CCA GCC ACT GCC AGC CAG) and XhoIR (CTG GCT GGC AGT GGC TGG CTC GAG CGT TTT CAC CTG ATC ATC GAC). For expression of the isolated Kbp LysM domain (residues 92-149) plasmid pIJ2 was engineered by the introduction of an NdeI site in *Kbp* from pAK1, digestion with NdeI to excise the NdeI fragment and religation of the vector with T4 DNA ligase after gel purification. Site directed mutagenesis of pAK1 to introduce an NdeI site was performed using the Stratagene quick change method with primers NdeIF (GTC GAT GAT CAG GTG AAA ACG CAT ATG CCA GCC ACT GCC AGC CAG) and NdeIR (CTG GCT GGC AGT GGC TGG CAT ATG CGT TTT CAC CTG ATC ATC GAC). Kbp-Bon_{His6} and Kbp-$LysM_{His6}$ were expressed in BL21(DE3) carrying plasmids pIJ1 and pIJ2, respectively, and purified as described for Kbp_{His6}. ^{15}N labelled proteins were expressed in BL21(DE3) grown in M9 minimal media with ^{15}N ammonium chloride as the sole nitrogen source.

NMR spectroscopy

Kbp_{His6} was expressed in *E. coli* grown in M9 minimal medium with (^{15}N-)ammonium chloride and ($^{13}C_6$-)glucose as sole nitrogen and carbon sources. Samples were prepared containing approximately 1 mM Kbp_{His6} and 5 mM KCl in 20 mM NaPi (pH 7.2). Resonance assignments were made using a combination of standard double and triple resonance spectra as described elsewhere (Ashraf et al., 2016) Structures were calculated using ambiguously assigned distance restraints derived from crosspeaks picked in 3D ^{13}C- and ^{15}N-editted NOESY-HSQC spectra (Marion et al., 1989; Vranken et al., 2005) recorded at 298 K. Phi and psi dihedral angle restraints for residues in regular secondary structure elements predicted by DANGLE (Cheung et al., 2010) were applied in the high temperature dynamics phases of each structure calculation and omitted during the final cooling stage. In the final iteration of the ARIA 2.3 (Habeck et al., 2004) driven calculations, a total of 5626

restraints were used to generate 100 structures from which an ensemble of the 20 structures which agree most closely with the experimental restraints was selected and refined in a full forcefield including explicit solvent (Linge et al., 2003). Structure quality parameters are summarised in Table 1. The structures and restraints are deposited in the protein data bank (PDB code 5fim).

Growth assays

To determine the effect of the addition of KCl into the growth media, cells were grown in a defined sodium phosphate media, NaM9, based on M9 minimal media with added KCl at the concentrations specified. The recipe for NaM9 salts per litre is $Na_2HPO_4.2H_2O$ 3.4 g, NaH_2PO_4 6.8 g, NaCl 0.5 g and NH_4Cl 1.0 g. 50 ml NaM9 salts were supplemented with $MgSO_4$, $CaCl_2$ and 2% glucose and inoculated with 0.5 ml of an overnight culture of wild-type or *Δkbp* BW25113 grown in LB broth. For experiments with added NaCl, cells were grown in standard M9 minimal media with additional NaCl as indicated.

Calorimetry

ITC experiments were performed on a VP-ITC microcalorimeter (MicroCal LLC, Northampton, MA, USA) in 50 mM Tris-HCl, 50 mM NaCl, pH 7.5 at 25°C with Kbp in the cell (cell volume = 1.4005 ml) and the MCl salts (where M is K^+, Cs^+, Rb^+, NH_4^+) in the syringe (10 mM). MCl was titrated into Kbp using an initial injection of 1 µl followed by 28 × 10 µl injections with stirring at 310 rpm. Prior to ITC measurements, proteins were dialysed overnight against the dialysis buffer used for protein heat of dilution control experiments. Data for Kbp-M^+ complex formation were fitted with a single site binding equation after correction for heat of dilution of using MicroCal ORIGIN software. The thermal stability of apo-Kbp and the Kbp-K^+ complexes was measured by differential scanning calorimetry (DSC) using a MicroCal VP-DSC (MicroCal LLC, Northampton, MA, USA) at a scan rate of 60°C h^{-1}. Samples were degassed briefly prior to loading in the DSC cell. Data were analysed using standard MicroCal Origin instrumental software.

Circular Dichroism

Near-UV CD spectra were acquired on a Jasco J-810 spectropolarimeter in 50 mM Tris 50 mM NaCl pH 7.5 ± 10 mM KCl at a protein concentration of 100 µM. Far-UV CD spectra were acquired in 20 mM Tris, 20 mM Na_2HPO_4, pH 7.5 ± 5 mM K_2HPO_4.

Stopped-flow fluorescence

Stopped-flow fluorescence experiments were performed on an Applied Photophysics stopped-flow spectrofluorimeter with a 1:1 mixing chamber. All experiments used an excitation wavelength of 280 nm with fluorescence monitored above 305 nm using a 305 nm cut-off filter. Entrance and exit slits were set to 0.7 mm. All experiments were performed in 50 mM sodium phosphate buffer pH 7.5 at 24.1°C. For experiments using NaCl, protein was dialysed into the sodium phosphate buffer with 0.3M or 0.6M NaCl overnight. A total of 5000 data points were collected over the course of each reaction, with 12 runs averaged for each association measurement.

The association of Kbp with K^+ was monitored under pseudo-first-order conditions. The concentration of Kbp (10 µM) was kept constant, varying the concentration of KCl dissolved in sodium phosphate buffer (0.5–1 mM) for 0.05 M and 0.3 M NaCl measurements, and between 0.5-20 mM KCl for the 0.6 M NaCl measurements. All data

were fitted with a single-exponential rate equation. Linear plots of k_{obs} were used to determine the bimolecular association rates for the complex formation.

Analytical ultracentrifugation

Sedimentation velocity experiments were carried out in a Beckman Coulter (Palo Alto, US) Optima XL-I analytical ultracentrifuge using an An-50 Ti eight-hole rotor. Kbp at concentrations ranging from 12 µM to 60 µM in 50 mM Tris, 50 mM NaCl, pH 7.5 was loaded into 12 mm path-length charcoal-filled epon double-sector centrepieces (360 µl per sample) and a 211 µM sample was loaded into a 3 mm path length centerpiece (90 µl) and spun at 49,000 rpm for approximately 9 h at 4°C. Scans were collected every 7 minutes using both interference and absorbance optics. The laser delay was adjusted prior to the run to obtain high-quality interference fringes. Absorbance data were acquired at 280 nm with a radial range of 5.8 - 7.2 cm and radial step-size of 0.005 cm. Kbp in 5 mM KCl supplemented buffer was analysed in exactly the same way. Data were analysed using SEDFIT (Schuck, 2000) to obtain the apparent sedimentation coefficients of Kbp ± K^+ using the continuous c(s) distribution model followed by fitting with the non-interacting discrete species model. The concentration dependence of the apparent sedimentation coefficients was then extrapolated to infinite dilution to determine the concentration-independent $s^0_{20,w}$. SEDNTERP (Laue et al., 1992) was used to calculate the partial specific volume (from the amino acid sequence of Kbp), the buffer density and viscosity at 20°C and 4°C.

Small angle X-ray scattering (SAXS)

SAXS was carried out on the X33 beamline at the Deutsches Elektronen Synchrotron (DESY, Hamburg, Germany). A range of concentrations (0.5-10 mg/ml) of Kbp with and without K^+, were loaded into the mica sample holders and data were collected. Scattering curves for buffer alone were recorded before and after each protein sample and an average of the buffer scattering was subtracted from the sample scattering. In the case of the K^+ bound form, the buffer was supplemented with 10 mM KCl. The logarithm of the scattering intensity, log I(q), was then plotted as a function of the scattering angle, q. The data obtained for each sample were analysed using PRIMUS and GNOM (Konarev et al., 2003; Svergun, 1992). The distance distribution function, p(r), was obtained by indirect Fourier transform of the scattering intensity, computed in GNOM, to look for changes in D_{max} (the maximum separation between scattering partners within the molecule) and more subtle conformational changes. A Guinier plot (ln I(q) vs q^2) was used to derive the radius of gyration, R_g, of Kbp, BON and LysM ± K^+ (Guinier, 1939).

Author contributions

K.U.A and B.O.S performed NMR analysis; I.J. and O.B. performed SAXS and AUC analysis; K.M., I.J., D.W. and S.M.K performed other biophysical analyses; D.W. performed microbiological work; B.O.S and D.W. conceived the work and wrote the manuscript with contributions from the other authors.

References

Ashraf, K.U., Walker, D., and Smith, B.O. (2016). NMR resonance assignments of Kbp (YgaU), an E. coli potassium binding protein. Biomol. NMR Assign.

Bateman, A., and Bycroft, M. (2000). The structure of a LysM domain from E. coli membrane-bound lytic murein transglycosylase D (MltD). J. Mol. Biol. *299*, 1113-1119.

Bernal-Cabas, M., Ayala, J.A., and Raivio, T.L. (2015). The Cpx envelope stress response modifies peptidoglycan cross-linking via the L,D-transpeptidase LdtD and the novel protein YgaU. J. Bacteriol. *197*, 603-614.

Bielnicki, J., Devedjiev, Y., Derewenda, U., Dauter, Z., Joachimiak, A., and Derewenda, Z.S. (2006). B. subtilis ykuD protein at 2.0 A resolution: insights into the structure and function of a novel, ubiquitous family of bacterial enzymes. Proteins *62*, 144-151.

Booth, I.R. (1985). Regulation of cytoplasmic pH in bacteria. Microbiol Rev *49*, 359-378.

Bossemeyer, D., Borchard, A., Dosch, D.C., Helmer, G.C., Epstein, W., Booth, I.R., and Bakker, E.P. (1989a). K+-transport protein TrkA of Escherichia coli is a peripheral membrane protein that requires other trk gene products for attachment to the cytoplasmic membrane. J. Biol. Chem. *264*, 16403-16410.

Bossemeyer, D., Schlosser, A., and Bakker, E.P. (1989b). Specific cesium transport via the Escherichia coli Kup (TrkD) K+ uptake system. J. Bacteriol. *171*, 2219-2221.

Bostick, D.L., and Brooks, C.L., 3rd. (2007). Selectivity in K+ channels is due to topological control of the permeant ion's coordinated state. Proc Natl Acad Sci U S A *104*, 9260-9265.

Brookes, E., Demeler, B., Rosano, C., and Rocco, M. (2010). The implementation of SOMO (SOlution MOdeller) in the UltraScan analytical ultracentrifugation data analysis suite: enhanced capabilities allow the reliable hydrodynamic modeling of virtually any kind of biomacromolecule. Eur. Biophys. J. *39*, 423-435.

Cheung, M.S., Maguire, M.L., Stevens, T.J., and Broadhurst, R.W. (2010). DANGLE: A Bayesian inferential method for predicting protein backbone dihedral angles and secondary structure. J. Magn. Reson. *202*, 223-233.

Doyle, D.A., Morais Cabral, J., Pfuetzner, R.A., Kuo, A., Gulbis, J.M., Cohen, S.L., Chait, B.T., and MacKinnon, R. (1998). The structure of the potassium channel: molecular basis of K+ conduction and selectivity. Science *280*, 69-77.

Gralla, J.D., and Vargas, D.R. (2006). Potassium glutamate as a transcriptional inhibitor during bacterial osmoregulation. EMBO J. *25*, 1515-1521.

Guinier, A. (1939). La Diffraction des rayons X aux très pétits angles: application à l'etude de phénomènes ultramicroscopiques. (Paris, Masson).

Habeck, M., Rieping, W., Linge, J.P., and Nilges, M. (2004). NOE assignment with ARIA 2.0: the nuts and bolts. Methods in Molecular Biology *278*, 379-402.

Koharudin, L.M., Viscomi, A.R., Montanini, B., Kershaw, M.J., Talbot, N.J., Ottonello, S., and Gronenborn, A.M. (2011). Structure-function analysis of a CVNH-LysM lectin expressed during plant infection by the rice blast fungus Magnaporthe oryzae. Structure *19*, 662-674.

Konarev, P.V., Volkov, V.V., Sokolova, A.V., Koch, M.H.J., and Svergun, D.I. (2003). PRIMUS: a Windows PC-based system for small-angle scattering data analysis. J. Appl. Crystallogr. *36*, 1277-1282.

Kuo, M.M., Saimi, Y., and Kung, C. (2003). Gain-of-function mutations indicate that Escherichia coli Kch forms a functional K+ conduit in vivo. EMBO J. *22*, 4049-4058.

Laue, T.M., Shah, B.D., Ridgeway, T.M., and Pelletier, S.L. (1992). Analytical Ultracentrifugation in Biochemistry and Biopolymer Science. In Analytical Ultracentrifugation in Biochemistry and Biopolymer Science, S.E. Harding, A.J. Rowe, and J.C. Horton, eds. (Cambridge, U.K.: Royal Society of Chemistry), pp. 90-125.

Lee, S.J., and Gralla, J.D. (2004). Osmo-regulation of bacterial transcription via poised RNA polymerase. Mol. Cell *14*, 153-162.

Linge, J.P., Williams, M.A., Spronk, C.A., Bonvin, A.M.J.J., and Nilges, M. (2003). Refinement of protein structures in explicit solvent. Proteins: Struct. Funct. Bioinform. *50*, 496-506.

Lockless, S.W., Zhou, M., and MacKinnon, R. (2007). Structural and thermodynamic properties of selective ion binding in a K+ channel. PLoS Biol. *5*, e121.
Marion, D., Driscoll, P.C., Kay, L.E., Wingfield, P.T., Bax, A., Gronenborn, A.M., and Clore, G.M. (1989). Overcoming the overlap problem in the assignment of 1H NMR spectra of larger proteins by use of three-dimensional heteronuclear 1H-15N Hartmann-Hahn-multiple quantum coherence and nuclear Overhauser-multiple quantum coherence spectroscopy: application to interleukin 1 beta. Biochemistry *28*, 6150-6156.
Medina, J., Catala, R., and Salinas, J. (2001). Developmental and stress regulation of RCI2A and RCI2B, two cold-inducible genes of arabidopsis encoding highly conserved hydrophobic proteins. Plant Physiol. *125*, 1655-1666.
Nakamura, T., Yuda, R., Unemoto, T., and Bakker, E.P. (1998). KtrAB, a new type of bacterial K(+)-uptake system from Vibrio alginolyticus. J. Bacteriol. *180*, 3491-3494.
Noskov, S.Y., and Roux, B. (2006). Ion selectivity in potassium channels. Biophys. Chem. *124*, 279-291.
Onufryk, C., Crouch, M.L., Fang, F.C., and Gross, C.A. (2005). Characterization of six lipoproteins in the sigmaE regulon. J. Bacteriol. *187*, 4552-4561.
Papanastasiou, M., Orfanoudaki, G., Koukaki, M., Kountourakis, N., Sardis, M.F., Aivaliotis, M., Karamanou, S., and Economou, A. (2013). The Escherichia coli peripheral inner membrane proteome. Mol. Cell. Proteomics *12*, 599-610.
Rai, N., Nöllmann, M., Spotorno, B., Tassara, G., Byron, O., and Rocco, M. (2005). SOMO (SOlution MOdeler): Differences between X-Ray- and NMR-Derived Bead Models Suggest a Role for Side Chain Flexibility in Protein Hydrodynamics. Structure *13*, 723-734.
Richey, B., Cayley, D.S., Mossing, M.C., Kolka, C., Anderson, C.F., Farrar, T.C., and Record, M.T., Jr. (1987). Variability of the intracellular ionic environment of Escherichia coli. Differences between in vitro and in vivo effects of ion concentrations on protein-DNA interactions and gene expression. J. Biol. Chem. *262*, 7157-7164.
Rocha, P.S. (2016). Plant abiotic stress-related RCI2/PMP3s: multigenes for multiple roles. Planta *243*, 1-12.
Roosild, T.P., Castronovo, S., Healy, J., Miller, S., Pliotas, C., Rasmussen, T., Bartlett, W., Conway, S.J., and Booth, I.R. (2010). Mechanism of ligand-gated potassium efflux in bacterial pathogens. Proc Natl Acad Sci U S A *107*, 19784-19789.
Sanchez-Vallet, A., Saleem-Batcha, R., Kombrink, A., Hansen, G., Valkenburg, D.J., Thomma, B.P., and Mesters, J.R. (2013). Fungal effector Ecp6 outcompetes host immune receptor for chitin binding through intrachain LysM dimerization. Elife *2*, e00790.
Schuck, P. (2000). Size-Distribution Analysis of Macromolecules by Sedimentation Velocity Ultracentrifugation and Lamm Equation Modeling. Biophys. J. *78*, 1606-1619.
Svergun, D. (1992). Determination of the regularization parameter in indirect-transform methods using perceptual criteria. J. Appl. Crystallogr. *25*, 495-503.
Svergun, D.I., Petoukhov, M.V., and Koch, M.H. (2001). Determination of domain structure of proteins from X-ray solution scattering. Biophys. J. *80*, 2946-2953.
Teriete, P., Yao, Y., Kolodzik, A., Yu, J., Song, H., Niederweis, M., and Marassi, F.M. (2010). Mycobacterium tuberculosis Rv0899 adopts a mixed alpha/beta-structure and does not form a transmembrane beta-barrel. Biochemistry *49*, 2768-2777.
Vijayakumar, S.R., Kirchhof, M.G., Patten, C.L., and Schellhorn, H.E. (2004). RpoS-regulated genes of Escherichia coli identified by random lacZ fusion mutagenesis. J. Bacteriol. *186*, 8499-8507.
Volkov, V.V., and Svergun, D.I. (2003). Uniqueness of ab initio shape determination in small-angle scattering. J. Appl. Crystallogr. *36*, 860-864.
Vranken, W.F., Boucher, W., Stevens, T.J., Fogh, R.H., Pajon, A., Llinas, M., Ulrich, E.L., Markley, J.L., Ionides, J., and Laue, E.D. (2005). The CCPN data model for NMR spectroscopy: Development of a software pipeline. Proteins: Struct. Funct. Bioinform. *59*, 687-696.

Weber, A., Kogl, S.A., and Jung, K. (2006). Time-dependent proteome alterations under osmotic stress during aerobic and anaerobic growth in Escherichia coli. J. Bacteriol. *188*, 7165-7175.
Weiden, P.L., Epstein, W., and Schultz, S.G. (1967). Cation transport in Escherichia coli. VII. Potassium requirement for phosphate uptake. J. Gen. Physiol. *50*, 1641-1661.
Yang, Y., Auguin, D., Delbecq, S., Dumas, E., Molle, G., Molle, V., Roumestand, C., and Saint, N. (2011). Structure of the Mycobacterium tuberculosis OmpATb protein: a model of an oligomeric channel in the mycobacterial cell wall. Proteins *79*, 645-661.
Yeats, C., and Bateman, A. (2003). The BON domain: a putative membrane-binding domain. Trends Biochem. Sci. *28*, 352-355.
Yim, H.H., and Villarejo, M. (1992). osmY, a new hyperosmotically inducible gene, encodes a periplasmic protein in Escherichia coli. J. Bacteriol. *174*, 3637-3644.
Yu, H., Noskov, S.Y., and Roux, B. (2010). Two mechanisms of ion selectivity in protein binding sites. Proc Natl Acad Sci U S A *107*, 20329-20334.
Zhou, Y., Morais-Cabral, J.H., Kaufman, A., and MacKinnon, R. (2001). Chemistry of ion coordination and hydration revealed by a K+ channel-Fab complex at 2.0 A resolution. Nature *414*, 43-48.

Table

Table 1. Parameters for the structure of Kbp determined by NMR spectroscopy. Average statistics were calculated from the 20 water-refined structures in the Kbp ensemble. The number of violations is shown as the average and standard deviation per structure.

NOE distance restraints	
NOE restraints	5626
Ambiguous	2741
Unambiguous, of which	2885
Intra-residue	1237
Inter-residue	
Sequential (|i-j|=1)	715
Medium-range (1<|i-j|<5)	371
Long-range (|i-j|≥5)	562
Violations per structure > 0.5 Å	0.05±0.218
Violations per structure > 0.3 Å	2.8±1.66
Distance restraint RMSD (Å)	0.023±0.001
Other restraints	
Dihedral angle restraints	162
Parameter RMSD from idealized geometry	
Bonds (Å)	3.9E-3±7.90E-5
Angles (°)	0.49±0.0097
Impropers (°)	1.39±0.057
[a,b]Coordinate RMSD (Å)	
Backbone heavy atoms	0.699±0.151
All heavy atoms	1.047 ±0.145
[b]Ramachandran statistics (%)	
Most favoured	84.3
Additionally allowed	13.0
Generously allowed	0.9
Disallowed	1.8

a, to the unbiased mean structure; b, residues 2-149

Figures

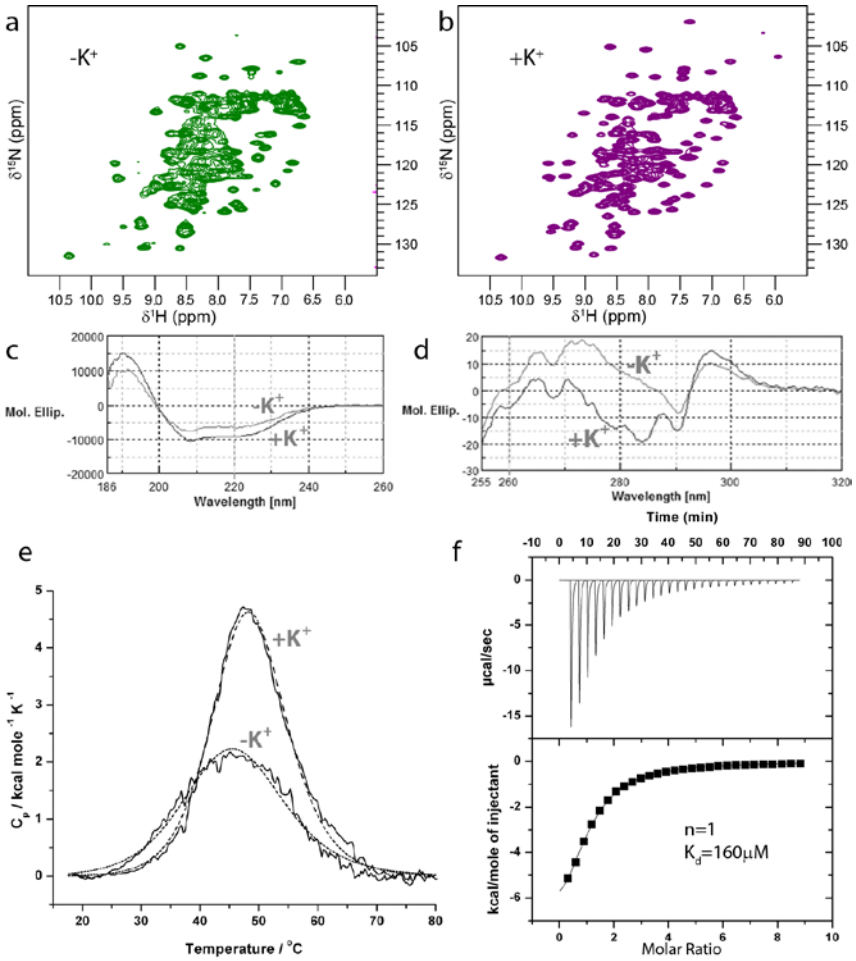

Figure 1. K^+ binding leads to stabilisation and structural changes in Kbp. ^{15}N HSQC NMR spectra of 200 µM Kbp in 20 mM NaPi, pH 7.2 in **a)** the absence, and **b)** the presence of 5 mM KCl. **c)** Near- and **d)** far-UV CD shows changes to secondary and tertiary structure of Kbp on K^+ binding. Near-UV CD was performed in 50 mM Tris 50 mM NaCl pH 7.5 ± 10 mM KCl at a protein concentration of 100 µM in a quartz cuvette of pathlength 0.5cm. Far-UV CD was performed at a protein concentration of 30 µM in 20 mM Tris, 20 mM Na_2HPO_4, pH 7.5 ± 5 mM K_2HPO_4 in a quartz cuvette of pathlength 0.02 cm. **e)** DSC shows Kbp is stabilised on binding K^+. Solid lines show experimental thermograms for Kbp in the presence and absence of K^+. Dashed lines show the fit with a 2-state unfolding model. Binding of K^+ gives rise to an increase in the T_m from 45.9 to 48.4°C and an increase in the enthalpy of unfolding from 50.2 to 77.8 kcal mol^{-1}. Experiments were performed in 50 mM Tris, 50 mM NaCl, pH 7.5 ± 1.27 mM KCl at a protein concentration of 64 µM. **f)** K^+ binding to Kbp monitored by ITC. The upper panel shows sequential heat pulses, after subtraction of dilution heats, on titration of KCl into Kbp in 50 mM Tris, 50 mM NaCl, pH 7.5 at 25°C. The lower panel shows integrated heat data fit with a one site binding model. These data show that Kbp binds a single K^+ ion and the equilibrium dissociation constant for the Kbp-K^+ complex is 161 µM (**Table S1**). See also Figure S1, S2 and S4.

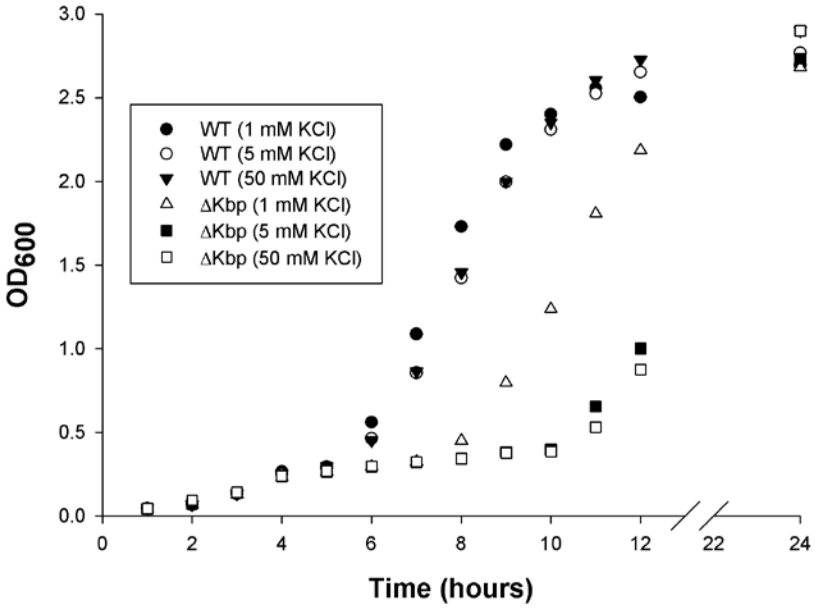

Figure 2. *E. coli* lacking Kbp show retarded growth at high concentrations of K^+. Wild-type and *⊿kbp E. coli* BW25113 cells were grown at 37°C in defined sodium phosphate based media with added KCl at 1, 5 and 50 mM. At higher K^+ concentrations (1, 5 and 50 mM) there was little variation in growth rate with K^+ concentration for the wild-type strain, however, the *Δkbp* strain showed a delay of around 2 hours in entering exponential phase at 1 mM KCl and around 5 hours at 5 and 50 mM KCl. See also Figure S3.

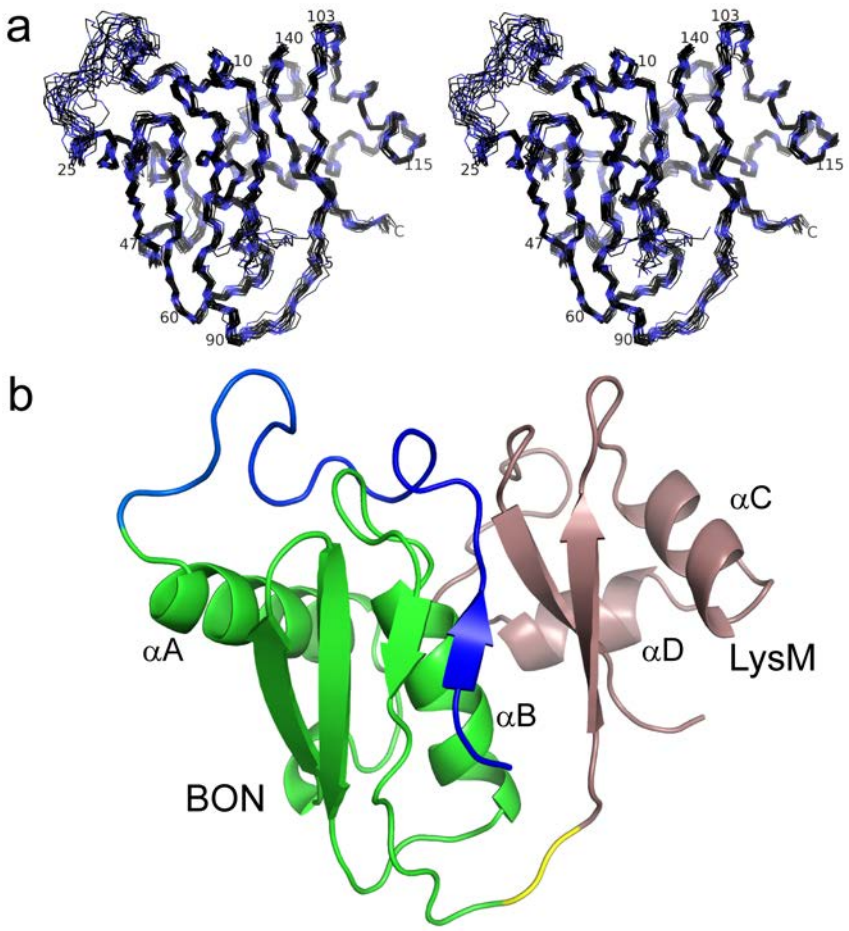

Figure 3. The structure of K^+ saturated Kbp. a) The ensemble of Kbp structures determined by NMR spectroscopy shown superimposed in backbone representation. The termini and a selection of residues are labelled and numbered. **b)** A cartoon representation of the Kbp structure with the BON and LysM domains coloured green and brown respectively. The N-terminal extension is shown in blue and the inter-domain linker in yellow.

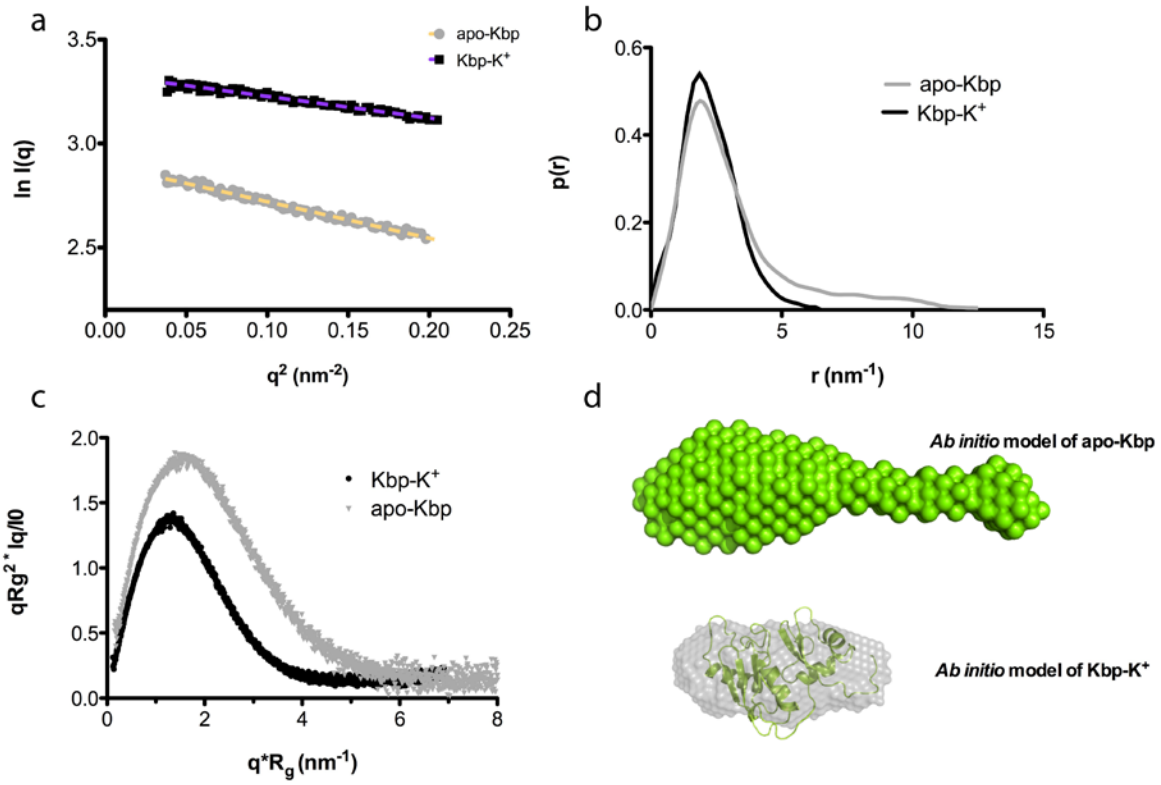

Figure 4. Conformational changes in Kbp on K^+ association determined by SAXS. a) Guinier analysis of apo- and K^+ -bound form shows a decrease in the radius of gyration (R_g) in the presence of K^+ as indicated by the reduced slope of the scattering intensity in the Guinier region of the SAXS curve. Extrapolation of the scattering intensity to zero concentration does not show any particule aggregation (data not shown) **b)** The distance distribution function for Kbp indicates a significant decrease in the maximum particle dimension (D_{max}) and a transition from an extended (12.5 nm) to a compact (6.2 nm) molecule in the presence of K^+. **c)** The normalised Kratky plot for Kbp in the presence of K^+ reveals single peak (black) with no obvious indications of flexibility, whereas the apo form of the protein (grey) exhibits a broader peak consistent with an increase in disordered content and an overall asymmetrical conformation, in accordance with the distance distribution function. **d)** The *ab initio* model of Kbp in the presence of K^+ overlaid with its NMR structure shows excellent agreement between the 2 structures. The apo-form of the protein exhibits an elongated shape in solution. See also Figure S5 and Table S2.

Supplementary Material

Supplementary Figures

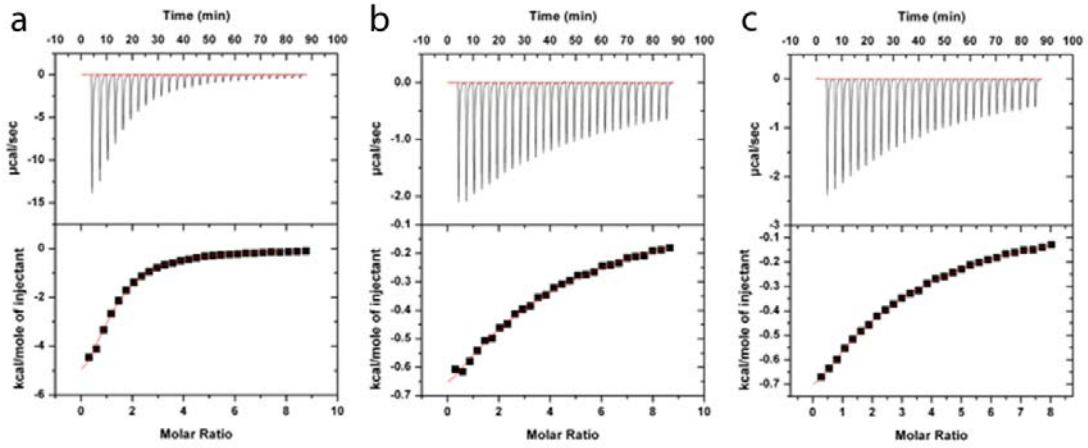

Figure S1, related to Figure 1. ITC data for a) Rb^+, b) Cs^+ and c) NH_4^+ binding to Kbp. Chloride salts of the respective cations were titrated into Kbp in 50 mM Tris, 50 mM NaCl, pH 7.5 as described in Materials and Methods. See Table S1 for derived parameters.

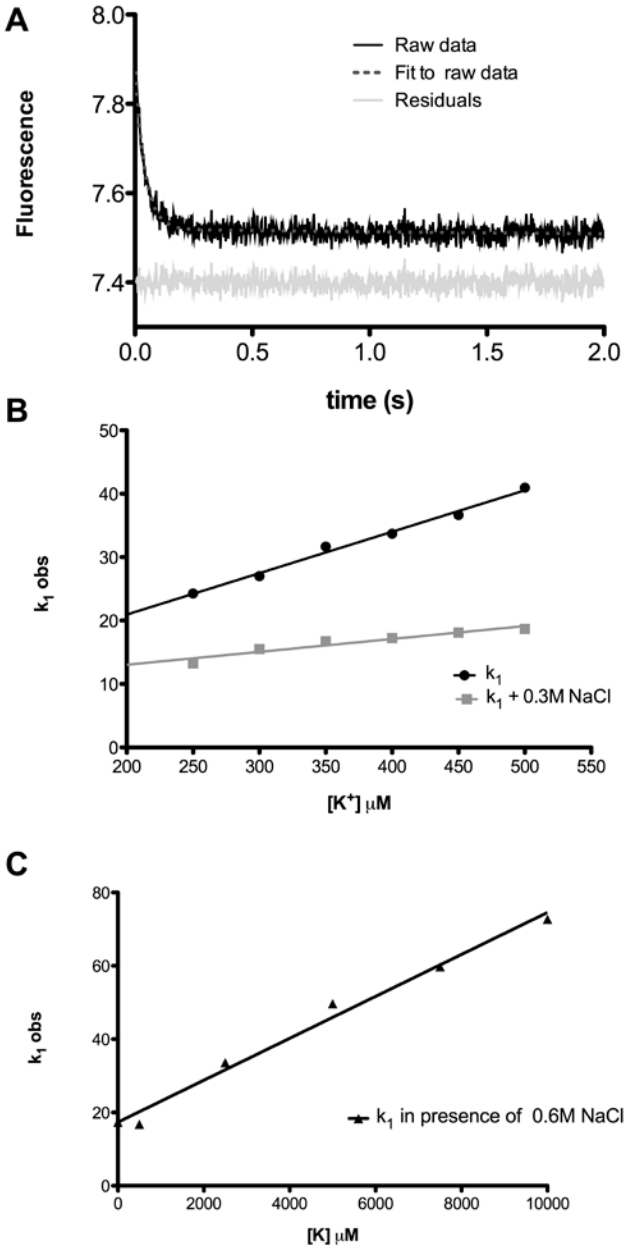

Figure S2, related to Figure 1. Association of Kbp and K^+ monitored by stopped-flow tryptophan fluorescence. a) Example stopped-flow trace under pseudo-first order conditions, with K^+ in excess fit by a single-exponential rate equation and residuals of fit shown. All experiments were performed in 50 mM sodium phosphate buffer pH 7.5 with NaCl added where indicated. Plot of k_{obs} vs K^+ concentration with b) 0 and 0.3 M added NaCl and c) 0.6 M added NaCl.

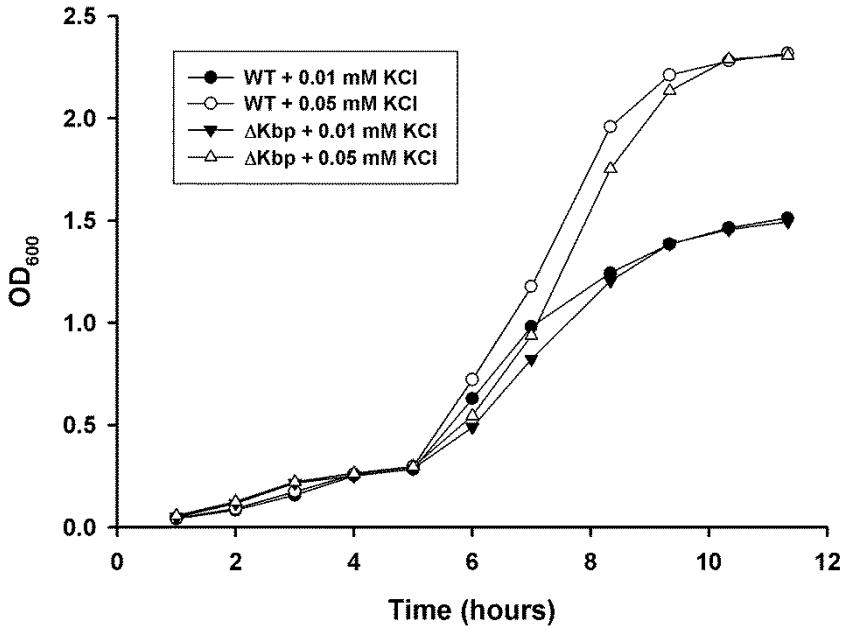

Figure S3, related to Figure 2. *E. coli* lacking Kbp show growth similar to the wild-type strain at low K^+ concentrations. Wild-type and *Δkbp E. coli* BW25113 cells were grown at 37°C in defined sodium phosphate based media with added KCl at 0.01 and 0.05 mM.

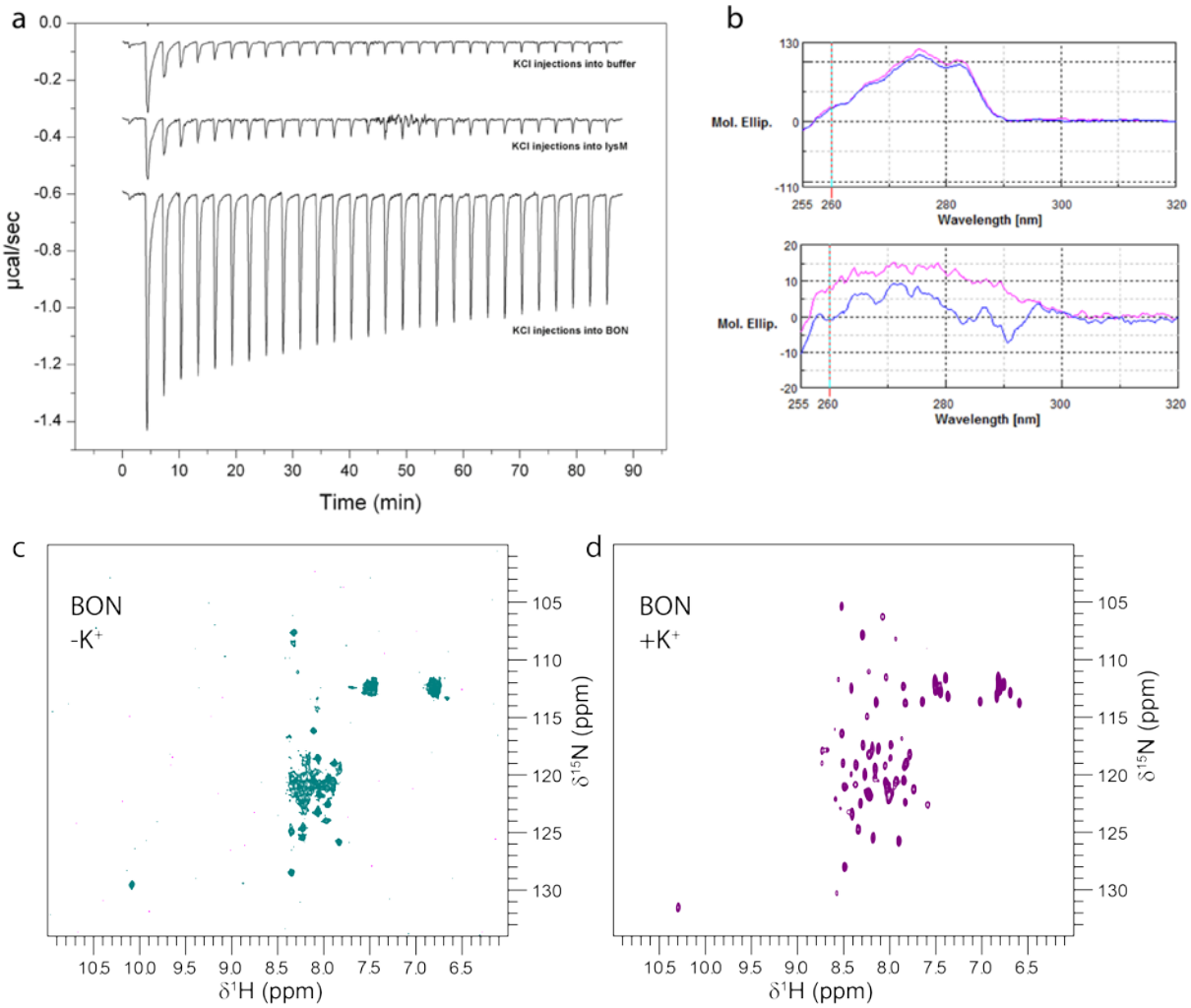

Figure S4, related to Figure 1. ITC, near-UV CD and NMR indicate that K^+ binds to the isolated BON domain of Kbp. a) ITC experiments show heat from sequential injections of KCl into buffer, isolated Kbp LysM domain and isolated Kbp BON domain. The excess heat generated on titration of KCl into isolated BON domain indicates binding. The shape of the curve indicates that this binding is weak and with an estimated K_d > 10 mM. **b)** Near-UV CD of K^+ binding to isolated LysM domain (top) and BON domain (bottom). c) Near-UV CD was performed in 50 mM Tris, 50 mM NaCl, pH 7.5 in the absence (pink) and presence (blue) of 10 mM KCl. **c) and d)** NMR indicates folding of the isolated BON domain on K^+ binding. ^{15}N HSQC NMR spectra of 100 µM Kbp BON domain (Kbp 1-89) in 20 mM NaPi, pH 7.2 in **c)** the absence and **d)** the presence of 270 mM KCl.

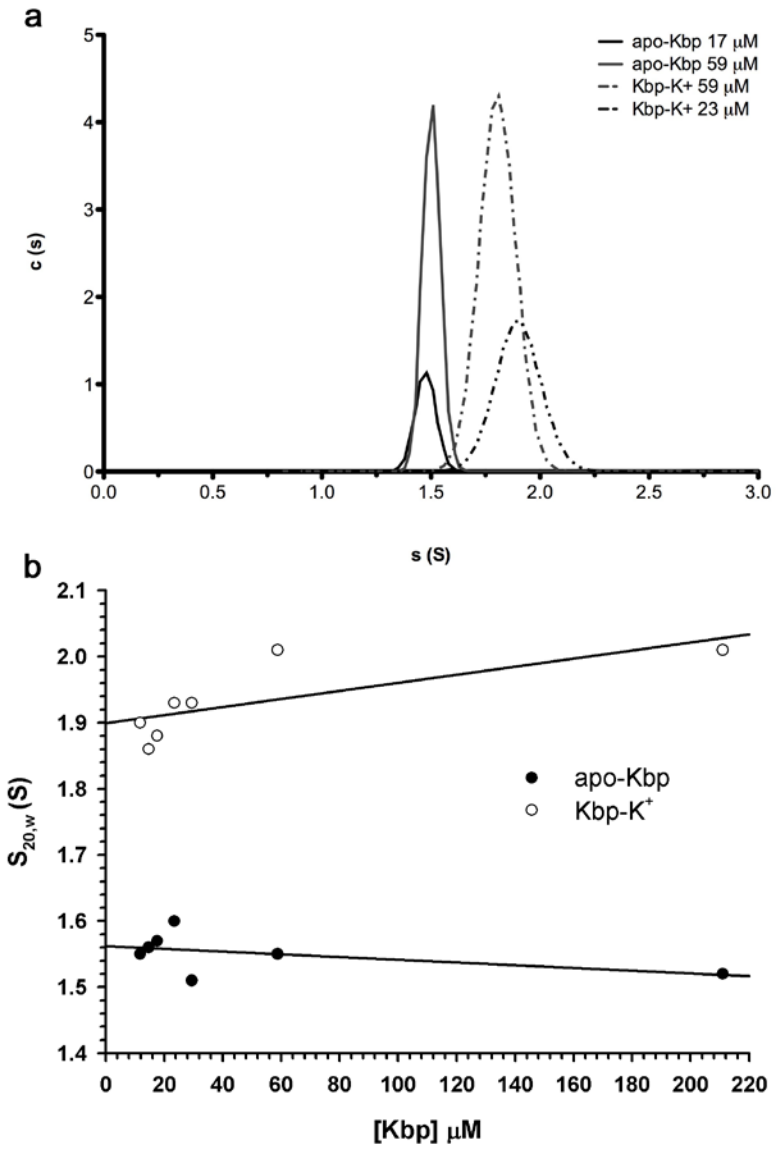

Figure S5, related to Figure 4. Sedimentation velocity experiments indicate that Kbp undergoes a large conformational change on K^+ binding. a) c(s) distributions derived via SEDFIT (Schuck, 2000) from SV data reveal a marked increase in apparent sedimentation coefficient upon K^+ binding to Kbp. Seven concentrations of Kbp both in the presence and absence of K+ were analysed with only two shown for clarity. **b)** Plot of apparent $s_{20,w}$ against concentration for apo-Kbp and Kbp-K^+. Concentration independent $s^0_{20,w}$ values were calculated by extrapolating the line of best fit to zero concentration, giving $s^0_{20,w}$ values of 1.56 S for apo-Kbp and 1.90 S for Kbp-K^+.

Supplementary Tables

Table S1, related to Figure 1. Thermodynamic parameters for ion binding to Kbp determined by ITC. Experiments were performed at 25°C. Errors shown are from duplicate experiments. For Cs^+ and NH_4^+ weak binding precluded accurate determination of thermodynamic parameters and only estimates of the K_d are shown. N is the stoichiometry of binding.

Ion	K_d (μM)	ΔH (kcal mol^{-1})	TΔS (kcal mol^{-1})	N
K^+	161 (±8)	9.8 (±0.2)	-4.6 (±0.2)	1.0 (±0.0)
Rb^+	225 (±43)	8.3 (±0.2)	-3.3 (±0.3)	1.0 (±0.1)
Cs^+	≈2000	ND	ND	ND
NH_4^+	≈1000	ND	ND	ND

Table S2, related to Figure 4. Experimental and calculated hydrodynamic parameters for apo-Kbp and Kbp-K^+. [a] $s^0_{20,w}$, R_g and f/f_0 were calculated using SOMO (**Brookes et al, 2010)** implemented as part of Ultrascan II (**Demeler, 2005**) for the dummy residue models derived from the SAXS data using GASBOR (**Svergun et al 2001**).

	apo-Kbp		Kbp-K^+	
	Experimental	**GASBOR[a]**	**Experimental**	**GASBOR[a]**
$s^0_{20,w}$ (S)	1.56	1.47	1.90	1.91
R_g (nm)	2.74	2.52	1.74	1.69
f/f_0	1.41	1.56	1.14	1.20